European Journal of Medicinal Chemistry 44 (2009) 3509–3518

Contents lists available at ScienceDirect

European Journal of Medicinal Chemistry

journal homepage: http://www.elsevier.com/locate/ejmech

Original article

Physicochemical properties and membrane interactions of anti-apoptotic derivatives 2-(4-fluorophenyl)-3-(pyridin-4-yl)imidazo[1,2-*a*]pyridine depending on the hydroxyalkylamino side chain length and conformation: An NMR and ESR study

Sébastien Follot [a], Jean-Claude Debouzy [a,*], David Crouzier [a], Cécile Enguehard-Gueiffier [b], Alain Gueiffier [b], Florian Nachon [c], Bertrand Lefebvre [d], Florence Fauvelle [a]

[a] *CRSSA, Unité de Biophysique, BP82, 38702 La Tronche Cedex, France*
[b] *PCMB EA 4244, Faculté de Pharmacie, 31 Avenue Monge, 37200 Tours, France*
[c] *CRSSA, Unité d'enzymologie, BP82, 38702 La Tronche Cedex, France*
[d] *CRSSA, Service de Biospectrometrie, BP82, 38702 La Tronche Cedex, France*

ARTICLE INFO

Article history:
Received 24 September 2008
Accepted 11 December 2008
Available online 10 January 2009

Keywords:
Imidazo[1,2-*a*]pyridine
Unilamellar vesicles
Multilamellar vesicles
Apoptosis
Nuclear Magnetic Resonance

ABSTRACT

Three imidazo[1,2-*a*]pyridine derivatives **3a**–**c** have been synthesized from p38 kinase inhibitor structures and evaluated as anti-apoptosis agents. These drugs were designed to interact with nucleic acids and membrane interactions by varying the chain length in position 6, from hydroxyethylamino (**3a**), to hydroxybutylamino (**3b**) and hydroxyhexylamino (**3c**). First experiments showed that **3a** and **3b** were insoluble in water while **3c** could be solubilized in water despite its partition coefficient (log $P = 3.2$). This latter feature was explained by the formation of a fifth intramolecular cycle thus allowing supramolecular structure formation (NMR and MD calculations).

The interactions with membranes have been studied using ^{1}H, ^{2}H, ^{31}P Nuclear Magnetic Resonance (NMR), Electron Spin Resonance (ESR) and High Resolution-Magic Angle Spinning (HR-MAS). Despite the insolubility of **3a** and **3b** in water, these derivatives could be partially solubilized by synthetic phospholipidic model membranes (small unilamellar vesicles, SUV). ^{1}H NMR paramagnetic broadening experiments performed on the same models showed that **3a** was located in the external layer, probably close to the surface while **3b** only formed external superficial adducts. Supplementary ^{31}P, ^{2}H NMR and ESR experiments on phospholipid dispersions confirmed the location of **3a** close to the polar headgroup of the external layer of the membrane, this resulting in a 2 K lowering of the transition temperature. Moreover, no significant interaction was detected on the deep part of the layer (^{2}H NMR and 16NS ESR experiments). This binding was also found in the presence of cell cultures, as revealed by HR-MAS NMR experiments.

Conversely, no significant interaction with membranes was found with **3b** or **3c**.

From both the unexpected solubility of **3c** and **3a** interactions with membranes, further chemical modifications were finally proposed.

1. Introduction

The association of inflammation process with cytokine induction (e.g. tumour necrosis factor (TNF) and interleukin-6 (IL-6)) [1,2] is now well admitted. Hence, high amounts of proinflammatory cytokines are observed in various pathologies involving autoimmune processes, such as toxic shock syndrome, diabetes, rheumatoid arthritis or osteoarthritis [3–6]. This led to an original therapeutic approach based upon the control and limitation of these proinflammatory cytokine levels (e.g. interleukin-1 (IL-1)) [7,8]. For instance, numerous intracellular kinase and

Abbreviations: 5 NS, 5-nitroxide stearate; 16 NS, 16-nitroxide stearate; CSA, Chemical Shift Anisotropy; DMPC, dimyristol phosphatidylcholine; MLV, multilayers vesicles; LPC, lysophosphatidylcholine; EPC, egg yolk phosphatidylcholine; SUV, unilamellar vesicles; ESR, Electron Spin Resonance; NMR, Nuclear Magnetic Resonance; HR-MAS, High Resolution-Magic Angle Spinning; MAPK, Mitogen-Activated Protein Kinase.

* Corresponding author. Fax: +33 (0)4 76 63 69 22.
E-mail address: jcdebouzy@crssa.net (J.-C. Debouzy).

0223-5234/$ – see front matter © 2008 Elsevier Masson SAS. All rights reserved.
doi:10.1016/j.ejmech.2008.12.026

phosphatase enzyme [9] inductions of cytokines have been extensively published [10,11]. Among them, an enzymatic protein, the p38 mitogen-activated protein kinase (MAPK) plays a crucial role in the signal transduction pathway leading to the production of proinflammatory cytokines: p38 MAPK activation is obtained by the phosphorylation of the tyrosin and tryptophan residues located in the regulatory loop between subdomains VII and VIII [12,13]. More than a single protein, the p38 MAPK family consists of 38 kDa proteins firstly identified in macrophages stimulated with lipopolysaccharide (LPS). However, besides its contribution to the inflammatory response and apoptosis promotion [14], the precise events leading to cell death are still partially unknown. Thus, the successive events called "MAPK cascade" [15], leading to the activation of p38 family, in fact results from the activation of MAPKKK4, and/or of the apoptosis signal-regulating kinase 1 (ASK1) [16] and/or TGF-activated protein kinase 1 (TAK1). These different kinases then activate the dual-specificity kinases MKK3, MKK4 and MKK6, the latter finally realizes the phosphorylation of p38 [17]. This step leads to the activation of p38 by inducing a conformational change, thus allowing substrates access to the activation loop [18,19]; p38 then plays a regulation role of the TNF expression. Besides, p38 activation allows the phosphorylation of several transcription factors, including ATF2 [11], NF-B, and MEF-2 that regulate mRNA expression. This led to the synthesis of p38 MAPK inhibitors as potential therapeutic agents in the treatment of inflammatory diseases.

Up to now, many different structures of p38 MAPK inhibitors have been synthesized and tested. For example, SB203580 and SB202190 are highly specific inhibitors of p38 MAP kinase and are extensively used as reference structures to probe p38 MAP kinase function in vitro and in vivo. From these basic structures, three imidazo[1,2-*a*]pyridine (Fig. 1) analogues have been synthesized as inhibitors of protein kinase (p38) [20–22]. The molecular basis was to obtain a direct competition with the binding of ATP on p38, by stabilizing a p38 conformation incompatible with ATP binding. Besides, the p38 MAPK inhibitors would also play a role in the apoptosis mechanism by the way of specific membrane interactions. Hence, beside chromatin condensation, nuclear or cytoplasmic fragmentation, and formation of dense bodies, numerous membrane changes [23], such as membrane blebbing, cell skrinkage have been observed [24–26].

Finally, the present work deals with two different aspects of the pharmacological properties of these drugs:

- In term of biodisponibility, to give an estimation of the physicochemical properties (solubility, membrane binding, possible supramolecular assemblies formation) after chain length and hydrophilic/hydrophobic balance modification (practically by chain length variation); the required log(*P*) and conformational studies in solution and ^{1}H NMR relaxation time measurements in solution are given.
- To study the location, and also the structural and dynamics consequences of the presence of the drugs in the membranes, by using synthetic phospholipidic systems and natural cell cultures and using spectroscopic NMR (^{1}H-, ^{2}H-, ^{31}P-, ^{1}H-HR-MAS NMR, and ESR methods) [27–31].

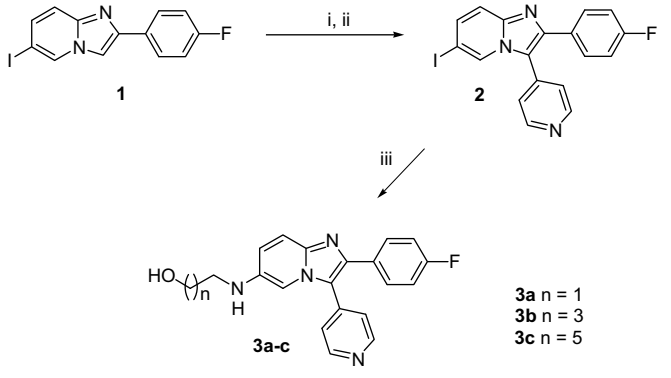

Fig. 1. Reagents and conditions: i) $ClCO_2C_2H_5$/pyridine for 5 h at RT, then o-chloranil/toluene for 3 h at RT, 47.5% yield; ii) aminoalcohol, CuI, K_3PO_4, ethylene glycol/butanol, for 14 h at 100 °C, 31–49% yields. Structures of compounds **3a**, **3b** and **3c**.

The final goal was to draw biophysical arguments to use versus the biological assays in order to obtain drug design guidelines for further syntheses.

2. Chemistry

Compounds **3a–c** were obtained in two steps starting from 2-(4-fluorophenyl)-6-iodoimidazo[1,2-*a*]pyridine **1** (Fig. 1). The pyridine ring was introduced in position 3 using ethyl chloroformate in pyridine at room temperature. An intermediate ethyl 1,4-dihydropyridin-1-ylformate was formed and treated with o-chloranil in refluxing toluene to give compound **2** in 48% yield. The introduction of the aminoalkylalcoo in position 6 was performed using a copper-catalyzed methodology in a sealed tube. The reaction was catalyzed by CuI in the presence of K_3PO_4 as base and ethylene glycol as ligand in butanol to provide **3a–c** in 31–49% yield (not optimized).

3. Investigations and results

3.1. Structure of the drugs in water

By considering the partition coefficients of the three compounds log *P* [**3a**] = 1.75; log *P* [**3b**] = 2.3; log *P* [**3c**] = 3.2, an increased solubility was expected from **3c** to **3a**. However, **3a** and **3b** were found completely insoluble in water (and 10 mM in $CHCl_3$, approximately). By the way of contrast, **3c** could be dissolved – even if sparsely (30 μM)– in water (and 6 mM in $CHCl_3$).

Hence, ^{1}H NMR lines were detected on the NMR aqueous sample containing 30 μM **3c** (Fig. 2-A). However, the linewidths measured (from 3 to 5 Hz) suggested that supramolecular assemblies had been formed, such as micelles or droplets [32]. This led to measure T_1 and T_2 relaxation times. These parameters are closely related to the correlation time τ_c and the volume of the system as described in the relations [33]:

$$1/T_1 = R_1 = A\cdot\tau_c\cdot\left[\left(1/\left(1+\omega^2\tau_c^2\right)+4/\left(1+4\omega^2\tau_c^2\right)\right)\right] \quad (1)$$

$$1/T_2 = R_2 = 6A\cdot\tau_c\cdot\left[4+9/\left(1+\omega^2\tau_c^2\right)+6/\left(1+4\omega^2\tau_c^2\right)\right] \quad (2)$$

with $\omega = 400$ MHz; $A = \gamma^4(h/2\pi)^2/r^6$; γ the gyromagnetic factor ($h/2\pi$) Planck's constant and r the inter spins distance.

Similar relaxation values were found within the molecule (T_2 ranged from 250 to 700 ms and T_1 from 0.6 to 1.2 s), thus giving an average T_1/T_2 ratio within 1.3–3 limits.

This allowed calculating the range of correlation time by using the ratio T_1/T_2 as follows:

$$T_2/T_1 = \left[1/\left(1+\omega^2\tau_c^2\right)+4/\left(1+4\omega^2\tau_c^2\right)\right]/ 6\left[4+9/\left(1+\omega^2\tau_c^2\right)+6/\left(1+4\omega^2\tau_c^2\right)\right] \quad (3)$$

relation in $\omega^2\tau_c^2$ simplified in a second degree equation giving $\omega\tau_c$ limits (≈ 0.16).

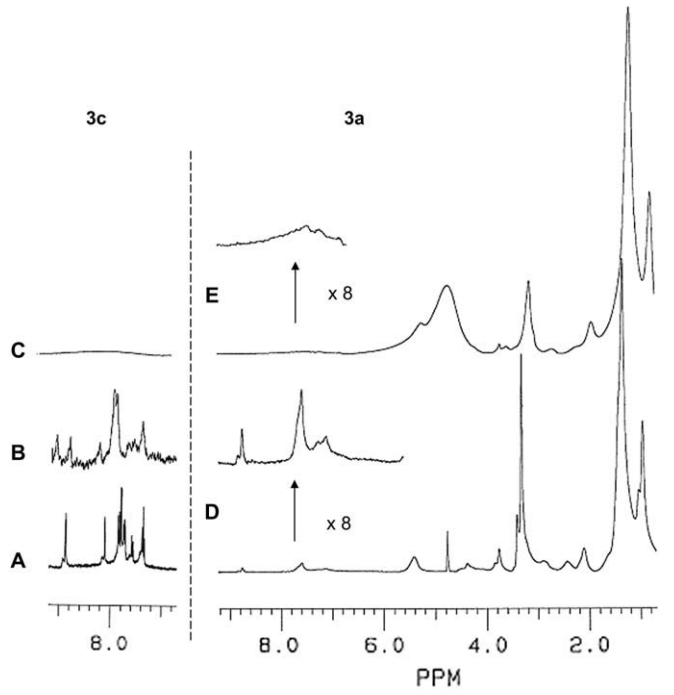

Fig. 2. ^{1}H NMR spectra of aromatic part of **3c** (left column) and experiments of **3a** (right column). A) pure in D_2O solution; B) and D) in the presence of SUV, drug/lipid ratio of 1/10; C) and E) after external addition of $MnCl_2$, 0.8 μM.

Then, using the spherical approximation for the molecular assembly, the Stokes–Einstein relation allows a coarse evaluation of the average apparent volume:

$$\tau_c = \eta V/kT, \text{ soit } V = kT\cdot\tau_c/\eta \quad (4)$$

where $\eta = 0.9\times10^{-3}$ P, (N s/m^2 at 298 K), $k = 1.38\times10^{-23}$ J/kg, $T = 297$ and V the volume (m^3). Finally, 0.8 nm^3 corresponding to an approximate 10 Å diameter. Such assemblies are significantly smaller than small unilamellar vesicles of phospholipids (typically of 10–20 nm radius, with T_1 in the 450–900 ms range and linewidths of 40–120 Hz) [30]. Due to the four heterocyclic rings of **3c**, stacking was probably present rather than spheric aggregates.

Fluorescence experiments were then undertaken to observe **3c** properties in a concentration range far below the minimum required for NMR experiments. It is well known that ring currents in heterocycles are strongly modified by stacking, resulting in absorption/emission spectra. As shown in Fig. 3, concentrations lower than 12 μM result in limited shifts both in maximum of absorption λe_{max} around 429 nm and absorption λa_{max} of 427 nm. Higher concentrations induce a significant jump in λa_{max} to 432 nm, then keeping relatively constant for higher concentrations. This feature is consistent with micelle formation or stacking, indicating a critical micellar concentration of 14 μM. This jump was relatively smoother for λe_{max}.

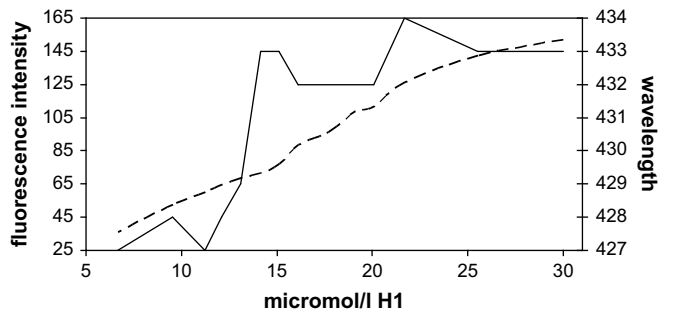

Fig. 3. Plot of the wavelength (—) and fluorescence intensity (– –) as a function of **3c** concentration (the range 6.6–30 μmol/L) in the distilled water.

Several arguments were also drawn from NMR dipolar correlation experiments (1Dnoe and noesy, not shown), summarized as follows:

Noe (%)	CH_2(OH)	H17/19 (8.77)	H16/20 (7.55)
CH_2(OH)	*X*	8	0
H(8.77)	6.7	*X*	10
H(7.55)	0	10	*X*

The distance (2.6 Å) between the two H16/20 and H17/19 protons was used as intramolecular reference to calculate CH_2(OH)–H17/19 distance and to set conformational simulation of **3c** molecule in the water (at p$D = 7$, where pyridine ring is protonated [p$K_a = 8$]). The result is shown in Fig. 4: a molecular dynamics simulation shows that the side chain forms of a fifth "pseudo" cycle resulting from interaction between the terminal hydroxyl and the pyridinium ring, especially if a supplementary water molecule is involved in an hydrogen bonding process and exposed to the surroundings.

Similar simulations performed with **3a** or **3b** failed to show any stable conformation, in agreement with the insolubility and precipitation of these molecules in water.

From this section, one can expect that the three derivatives exhibit quite different interactions with biological barriers. Hence, both solubility and cell membrane crossing are evident limiting factors in terms of biodisponibility, especially when the pharmacological final target is supposed to be intracellular, proteins or nucleic acids. These interactions are the topic of the next sections.

3.2. Interactions with membranes

3.2.1. Membrane binding/solubilization

3.2.1.1. Cell cultures. A first test was performed by recording ^{1}H NMR spectra of cell cultures in the presence of **3a**, **3b** or **3c** after strong vortexing of the NMR tube. As shown in Fig. 5, cell resonances of washed THP-1 (40 M cells/mL in PBS) are easily detected. After addition of **3a** (10 mM), supplementary resonances are identified in the aromatic part of the spectrum (8.8–7 ppm); despite broadened to 4–5 Hz, these resonances are similar to those of **3a** (in $CDCl_3$). As **3a** was completely insoluble in water, this

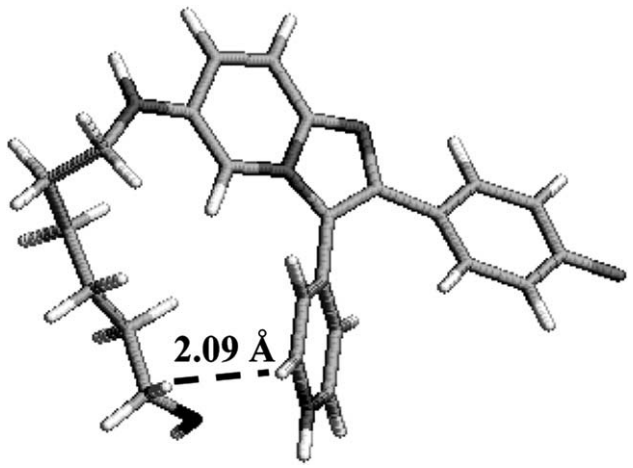

Fig. 4. 3D structures of **3c** after minimization and molecular dynamics simulation using the MM2 force field of Chem3D Ultra (CambridgeSoft).

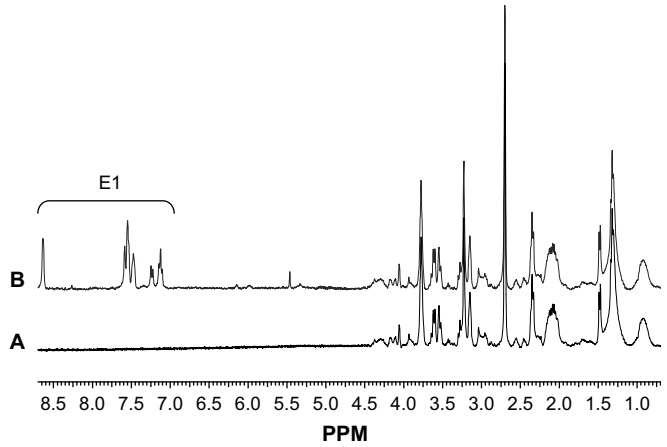

Fig. 5. 0.7–8.7 ppm region of ^{1}H NMR spectra (9.4 T), A) of THP-1 (40 M cells/mL), B) in the presence of **3a** (0.5 mM) (The water signal was removed using the ACDLABS 10.0 software).

feature indicated that this compound was at least partially solubilized by –or bond to– the cells. This was confirmed by recording noesy experiments that showed a dipolar connectivity between the **3a** peak labeled H-5 (7.5 ppm) and a cell group of resonances around 3.2 ppm ($-N(CH_3)^+_3$).

This was not the case for **3b** (not shown): both the complete absence of supplementary resonance on the cell spectrum, and the observation of a precipitate on the bottom of the sample ensured the absence of significant interaction with THP-1 cells.

As **3c** was soluble in water, no data of interest was drawn from the same experiment; however, the chemical shift of **3c** resonances in the presence of cells was very close to those detected in water, suggesting that **3c** was still in an aqueous environment.

Complementary information was then drawn by using synthetic small unilamellar vesicles (SUV) as model mimicking the biological membranes.

3.2.1.2. Small unilamellar vesicles. In order to study the location of drugs in membranes, we used sonicated unilamellar vesicles as a membrane model. Such a system gives relatively narrow lines so that one can expect to detect the drug resonances at high field.

Drug locations in membrane shows the 400 MHz ^{1}H NMR spectrum of SUV in the presence of drug (drug of lipid ratio $R = 1/10$). Fig. 2 shows the aromatic part of ^{1}H NMR spectra for the different drugs **3a** (right D, E) and **3c** (left A, B, C), **3b** giving quite similar results as **3c**. As expected from the chemical structure, all these compounds present a very good solubility in $CDCl_3$ giving typical linewidths narrower than 1 Hz. Compared to **3c**, **3a** and **3b** were completely insoluble in water, but at least partially solubilized by –or bond to– SUVs. As **3c** was already soluble in water (Fig. 2-A), but the chemical shift values of all the **3c** signals are close to those found in water. As far as the linewidths are concerned, **3a** and **3b** resonances in SUV are broadened by comparison with their spectrum in $CDCl_3$. Compared to phospholipid resonances, the linewidths of drug resonances are close to those observed for the protons of the most mobile part of the phospholipids molecule, i.e., the extremities.

In order to precisely locate the drug molecules in the bilayer, we added paramagnetic manganese ions to drugs-containing SUV (Fig. 2-C,E). As a reminder addition of $MnCl_2$ (paramagnetic molecule), broadens the resonances of geometrically accessible proton of the external layer of the vesicles, e.g. the polar choline headgroup. Under these conditions, the spectra recorded on the same systems show a dramatic broadening of **3a** resonances (Fig. 2-E), while the paramagnetic effect is stronger for the other drugs. This feature indicates that **3a** is both mobile and located close to the superficial part of the layer, while the spectra of **3b** and **3c** indicate embedding in the membrane.

3.2.2. Multilayer vesicles

3.2.2.1. Acyl chain level on phospholipids dispersions

3.2.2.1.1. ^{2}H NMR of chain-perdeuterated DMPC liposomes. ^{2}H NMR line shape: The spectrum of DMPC-d_{54} dispersions (DMPC with perdeuterated chain) is typical of phospholipid bilayers in the liquid crystal phase (temperature of 313 K, as shown on the partially dePaked spectrum) [35,36]. Such a spectrum appears as a superimposition of symmetrical doublets, each doublet corresponding to a methylenic CD_2 group of the acyl chain. For a given doublet, the splitting (quadrupolar splitting, $\Delta\nu_Q$) is directly related to the local order following the relation:

$$\Delta\nu_Q = \left[A\left(3\cos^2\theta - 1\right)\right]/2$$

where A is 170 kHz (for CD_2 bound in DMPC) and θ is the averaged value of the solid angle of reorientation. This splitting can be used in a first approximation as an order parameter. As the acyl chain fluidity decreases from the terminal methyl group (CD_3) to the methylenic groups close to the polar head of the lipids (the so-called "plateau region", from C-2 to C-8 of the chain), the resulting spectrum consists of *i*) an inner doublet with a quadrupolar splitting (in the 2–4 kHz range depending on temperature) attributed to the CD_3 methyl group *ii*) doublets with increasing quadrupolar splittings assigned to successive CD_2 groups from C14 to C9; *iii*) the external edge doublet, attributed to the deuterium of the C2–C8 plateau region where quadrupolar splitting is measured between 24 and 30 kHz.

The main spectra recorded under the same conditions in the presence of **3c** or **3b** (up to $R = 1/5$ m/m) were super imposable upon those of DMPC-d_{54}, both in quadrupolar splittings and in main linewidths over the whole temperature range observed (294–313 K). This can be observed in the plots Fig. 6 of CD_3 and Plateau region splittings, and also on the fluidity profile draw in Fig. 6-A (lower left trace). This was also the case in the presence of **3a** for CD_3 (Fig. 6-B) and CD_2 doublets down to the position C8. Conversely, the fluidity profile built from the position 8 to the plateau resonances showed a progressive increase in the fluidity in the presence of **3a**; furthermore, plateau resonance splittings exhibited the most significant reductions in the low temperature domain (up to 2 kHz at 298 K), whereas the transition temperature was unchanged (297 K).

3.2.2.1.2. ESR experiments. Spin label experiments were then realized to investigate the membrane fluidity in different temperature conditions. Two probes were separately used, 5 NS gate information about superficial membrane fluidity, while 16 NS concerned the inner membrane region.

The overall result (Fig. 7) shows an increase in the mobility of the two probes contribution in all groups as temperature increases. As previously described in MLV model [37], the phase transition in control groups occurs near 297 K.

5 NS results are drawn from Fig. 7-A. A drop in the order parameter could be observed between **3a** group and the other group. This shift was only noticed around the transition phase at 296 and 297 K **3b**, **3c** and control group provided similar lines.

These results were not observed at the inner compartment of the membrane.16 NS results fail to show any difference for the rotational correlation time of the probe between groups at all temperatures (Fig. 7-C).

These features indicate that **3a** induce a slight increase in membrane fluidity specifically located at the external compartment of the bilayers.

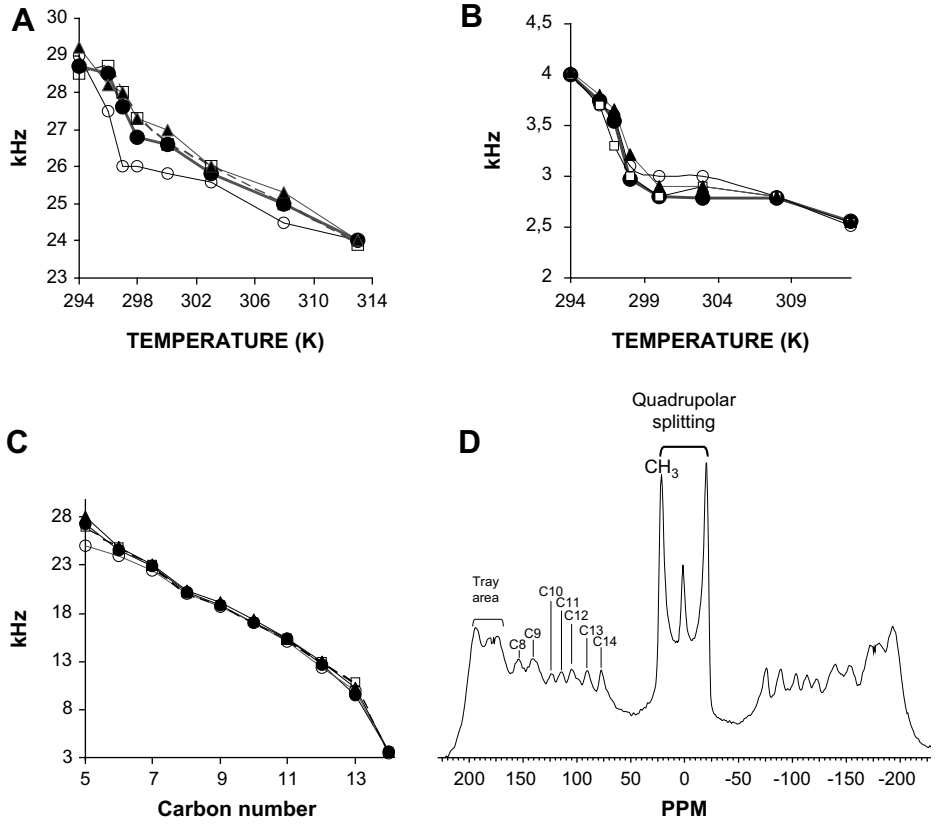

Fig. 6. Top traces temperature dependence of the half quadrupolar splitting (kHz) for pure DMPC (▲), and in the presence of **3a** (○), **3b** (●), **3c** (□), for plateau resonances (A) and terminal CD_3 group resonances (B); **Bottom traces** carbon number of the half quadrupolar splitting (kHz) for pure(▲), and in the presence of **3a** (○), **3b** (●), **3c** (□); ^{2}H NMR spectrum of (D) pure DMPC-d_{54} dispersions at 296 K.

3.2.2.2. Polar headgroup level

3.2.2.2.1. ^{31}P NMR of DMPC phospholipid dispersions (MLV). The bottom trace presented in Fig. 8-B is representative of axially symmetric powder phosphorus spectrum of standard bilayer structures of DMPC below phase transition [38]. The temperature dependance of ^{31}P Chemical Shift Anisotropy (CSA, figured by an horizontal bar) was measured on the phosphorus-NMR spectra of multilayers (MLV) [39] of pure DMPC or in the presence of **3a**, **3b** or **3c** (see legend of Fig. 8-A). As classically admitted [40], CSA value can be considered as representative of the fluidity of the superficial part of a membrane, where phosphorus nuclei are located. By comparison with DMPC, no significant modification in the line shape was detected on the spectra of MLV containing **3b** or **3c** (under the same experimental conditions) indicating that the main bilayer structure is not clearly modified. Hence, no resolved resonance indicative of detergent effect was observed at the isotropic position. As neither the intensity ratio of $\sigma^{\parallel}/\sigma^{\perp}$, nor typical linewidth of $\sigma^{\perp}$ resonance was modified, membrane (re)orientation or change in local motion was also refuted. Furthermore, in the presence of **3c** or **3b**, the plots presented in Fig. 8-A are consistent with a gel/liquid crystal phase transition around 297 K, and CSA values in the 294–313 K range very close to those of pure DMPC. It clearly appears that the temperature of transition gel–liquid crystal (297 K) is not modified in the presence of these drugs.

By the way of contrast, a significant reduction of the CSA measured in the presence of **3a** occurred in the low temperature domain, 294–298 K (295 K, see Fig. 8-A, the top trace of drug/lipid 1/5 W/W). Besides, the phase transition temperature was found to be 2 K lower than that of pure DMPC, whereas the traces recorded at higher temperature (298–313 K) did not significantly differ from those of pure DMPC.

Finally, the temperature dependence of ^{1}H NMR HR-MAS spectra was measured on MLV of pure DMPC or in the presence of **3a**, **3b** or **3c** (not shown). The gel/liquid crystal phase transition was deduced from the half-widths of multilayer resonances (MLV). These experiments confirmed the reduction of 2 K of transition temperature of **3a**.

This feature supports that **3a** interacts with the superficial part of the membrane where phosphorus is located, while **3b** or **3c** do not. Further arguments were obtained by recording ^{2}H NMR spectra on choline γ-methyl perdeuterated MLV in the presence of **3a**.

3.2.2.2.2. ^{2}H NMR of choline-deuterated DMPC liposomes. As the 3 γ-methyl groups of choline are magnetically equivalent, the spectrum of pure DMPC (Fig. 8-D, top) consists of two spectral components: an isotropic line resulting from the remaining protons of the solvent, thus freely moving. Besides, the contribution of methyl groups is a single doublet, which quadrupolar splitting (QS) is indicative of local fluidity: as plotted in Fig. 8-C, a jump in QS is observed at transition temperature. That is not the case in the presence of **3a** (Fig. 8-D bottom, 300 K): only a progressive decrease of QS is observed with increasing temperature, thus revealing a complete absence of structure transition of the membrane, while a limited increase in local order is observed (maximum difference of 50 Hz at 300 K). Conversely, there were no differences in the presence of **3c** or **3b** (not shown).

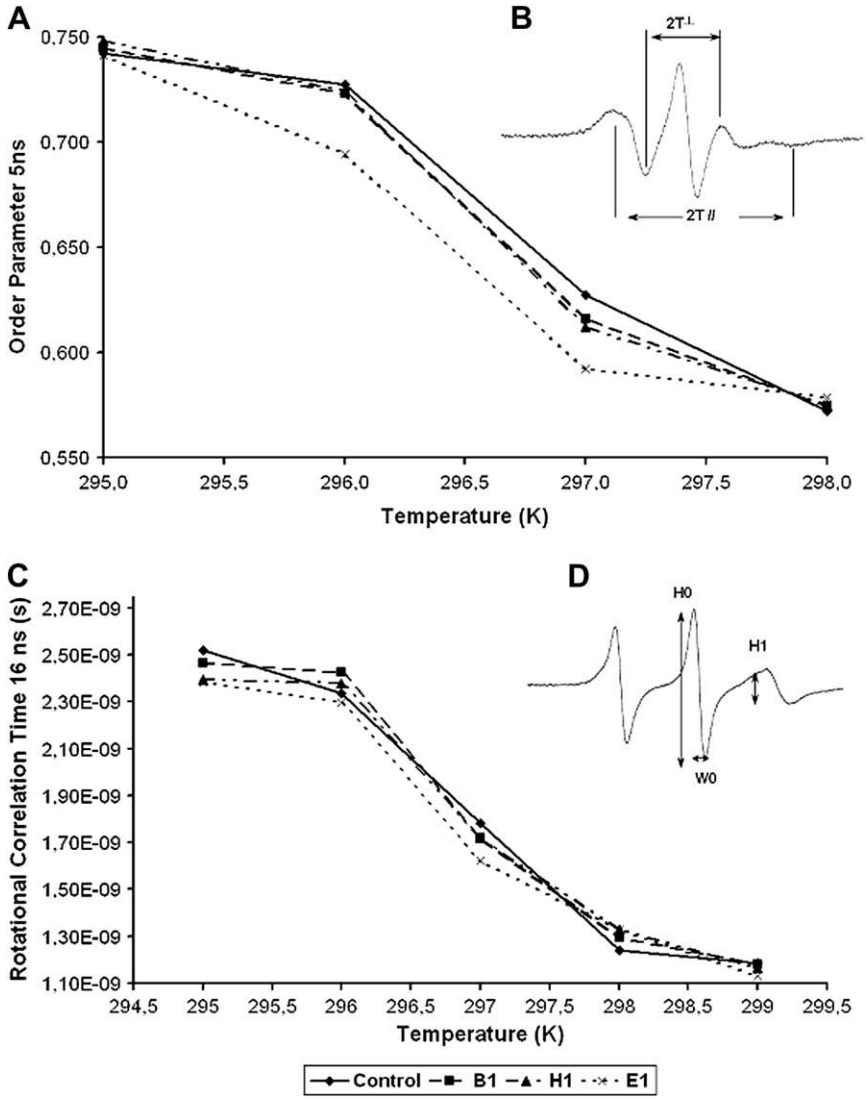

Fig. 7. ESR spin labeling experiment: A) Temperature dependence of the order parameter (5 NS) for pure DMPC and in the presence of **3a**, **3b**, **3c**; B) Typical 5 NS spectrum parameter used for order parameter estimation are inner ($2T_{\perp}$) and outer hyperfine ($2T_{\parallel}$) splitting; C) Temperature dependence of the rotational correlation time (16 NS) for pure DMPC and in the presence of **3a**, **3b**, **3c**; D) Typical 16 NS spectrum, parameter used for rotational correlation time was central peak intensity H_0, High field peak intensity and the with of the mid-field line W_0.

The involvement of the polar head was also investigated by recording ^{1}H NMR spectra of **3a** in the presence of glycerophosphatidylcholine solution (GPC). As the sole resonances of GPC could be detected, it was concluded that the polar head could not by itself build a stable association with **3a** (**3a** finally precipitated in the NMR tube).

Finally, micelles of lysophosphatidylcholine (LPC) successfully dissolved **3a**, and a weak dipolar correlation was found between the protons Ph-2,6, H-8 ($\delta = 7.6$ ppm) from **3a** and the CH ($\delta = 5.6$ ppm) resonance of LPC glycerol (not shown).

4. Discussion

The present work investigates the physicochemical properties and membrane interactions of alkylated derivatives of imidazo[1,2-*a*]pyridine, structural analogous of p38 kinase inhibitors. The poor solubility of the reference structures (SB203580 and SB202190) limits their biodisponibility so that large amounts of drugs are required to obtain the desired biological effect. The three derivatives in this study were designed to obtain a range of amphiphilic properties (log *P* from 1.75 to 3.2) without altering the basic imidazo[1,2-*a*]pyridine structure. Their observed properties, draw arguments for further chemical modifications.

The first unexpected result was the insolubility of **3a** and **3b**, compared to the relative solubility of **3c** that ran counter the log *P* values of these molecules; this solubility was found to be related to the formation of a fifth "pseudo" cycle by intramolecular interactions. Classically, polycyclic aromatic molecules tend to stack to minimize their contact with water [41]. Due to the hexyl chain length, chain reorientation occurred, as ascertained by noe experiments and MD calculations. The formation of this fifth pseudocycle resulted in a more rigid structure, favorable to stacking, as proved by relaxation measurement experiments. Conversely, the relatively free motion of butyl or ethyl chains precluded such molecular packing. This demonstrates the importance of the chain length present in position 6.

In the drug design process, the choice of chemical modifications starting from a basic structure can also be guided by the nature of the expected target as well as the pathway that will be used to

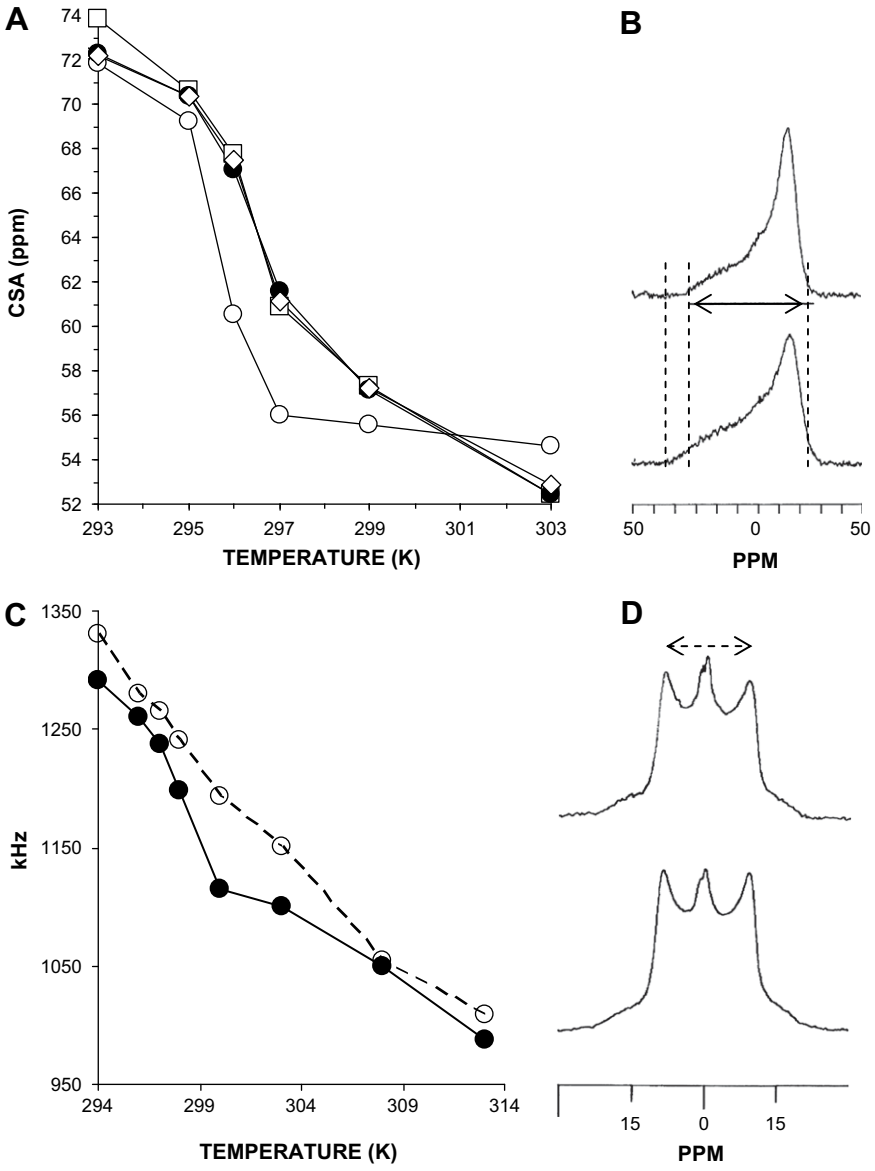

Fig. 8. ^{31}P NMR (top) of DMPC and ^{2}H NMR (bottom) of DMPC-d_9 : A) Temperature dependence of the Chemical Shift Anisotropy for pure DMPC (□),and in the presence of **3a** (○), **3b** (◇), **3c** (●); B) Typical spectrum of (top) DMPC bilayers (50 mM) close to transition temperature (296 K) (bottom) and in the presence of **3a** (drug/lipid 1/5 W/W); C) Temperature dependence of the quadrupolar splitting (kHz) for pure DMPC (●), and E1/DMPC systems (drug/lipid 1/5 W/W) (○); **D**) To show the splitting of CD_3 groups of DMPC (top) and in the presence of **3a** (bottom).

reach this target and overcome natural barriers. However, it was worth to note that the only interaction observed with the cell membrane was obtained with **3a**. As the molecular target (p38 kinase) is located in the intracellular compartment it was important to study the interactions of the drugs with the cellular barriers, i.e., the membranes. Moreover membrane fluidity changes have been clearly evidenced during apoptosis [42,43].

The studies performed with unilamellar model membranes (SUV) showed that **3a** interacts with the superficial part of the membrane layer. In contrast, no incorporation or binding could be observed for the other drugs in this membrane model. This feature was in agreement with the rather amphiphilic properties of **3a** and led us to further investigate the nature of the interactions with membranes. The ^{31}P NMR spectra and ^{2}H NMR patterns obtained from DMPC-d_{54} and DMPC-d_9 dispersions proved that **3a** was truly located in the external layer of the membrane, close to the polar headgroup (noe with glycerol proton in LPC micelles, and variations in the quadrupolar splitting of γ-perdeuterated choline in DMPC dispersions). This fluidization was also noted on the methylenic groups of the plateau region on chain-perdeuterated experiments, and confirmed by ESR experiments using superficial labeling probes. This interaction resulted in a lowering of the main temperature transition of 2 K in DMPC models.

5. Conclusion

The present work highlights two major points in the design of bioavailable derivatives:

- An improved solubility in the biological medium could be achieved by choosing 6-atom chain length intramolecular

interactions leading to a more rigid structure and soluble spheric aggregates;
- Enhancement of membrane interactions/penetration could be achieved by hydroxyl substitutions (1 and/or 2 groups) on the C6 lateral chain.

These propositions are currently tested in current syntheses.

6. Experimental section

6.1. Chemistry

The melting points were determined in a capillary apparatus and are uncorrected. The NMR spectra were recorded on spectrometer Bruker AM 400 WB or AVANCE-DMX-400 instruments and chemical shifts are expressed in ppm relative to trimethyl silyl propionic acid sodium (TSP) from residual $CHCl_3$ at δ 7.3 (^{1}H) and central resonance of $CDCl_3$ at δ 77.1 (^{13}C). The NMR spectra of compound **1** were performed at 200 MHz (^{1}H) and 50 MHz (^{13}C) in $CDCl_3$ or DMSO-d_6 on Bruker DPX 200 instruments. Signals are described as singlet (s), broad singlet (bs), doublet (d), triplet (t), quartet (q) and multiplet (m). Possible inversion of two values in the NMR spectra is expressed by an asterisk. Elemental analyses (C, H, N) were within $\pm$ 0.4% of theory. 2-(4-Fluorophenyl)-6-iodoimidazo[1,2-*a*]pyridine **1** was prepared by a multistep synthesis previously reported in the literature [44].

6.1.1. 2-(4-Fluorophenyl)-6-iodo-3-pyridin-4-ylimidazo [1,2-a]pyridine (**2**)

To a solution of 6-iodo-2-(4-fluorophenyl)imidazo[1,2-*a*]pyridine **1** (3 g, 8.9 mmol) in 7.6 mL of pyridine (7 g, 88.8 mmol) were added dropwise 4.8 mL of ethyl chloroformate (4.8 g, 44.4 mmol) at a temperature comprised between 0 and 5 °C. After 3 h of stirring at room temperature, the same volumes of pyridine and ethyl chloroformate were again added to the cooled reaction mixture. After 2 h of stirring, the suspension was treated with 100 mL of water and extracted with 100 mL of DCM. The organic layer was washed three times with water and dried over anhydrous $MgSO_4$. After concentration, the residue was dissolved in 20 mL of toluene, added of o-chloranil (2.2 g, 8.9 mmol) and stirred at room temperature for 3 h. The reaction mixture was then neutralised with an aqueous solution of NaOH 2 N and extracted with DCM. The organic layer was dried over anhydrous $MgSO_4$ and concentrated to dryness. The residue was chromatographed on silica gel eluted with DCM–methanol (99–1) (1.75 g). Yield: 47.5%. Mp = 240 °C. ^{1}H NMR (200.13 MHz, $CDCl_3$): 8.85 (d, J = 5.8 Hz, 1H, Pyr-2, 6), 8.32 (m, 1H, H-5), 7.59 (dd, J = 9–5.4 Hz, 2H, F-Ph-2,6), 7.56 (d, J = 9.6 Hz, 1H, H-8), 7.54 (dd, J = 9.6–1.4 Hz, 1H, H-7), 7.42 (d, J = 5.8 Hz, 2H, Pyr-3,5), 7.06 (t, J = 9 Hz, 2H, F-Ph-3,5). ^{13}C NMR (50 MHz, $CDCl_3$): 163.2 (J = 247 Hz, C–F), 151.7 (C–H), 144.5 (C), 143.9 (C), 137.7 (C), 134.0 (C–H), 130.57 (J = 8 Hz, C–H), 129.4 (C), 128.22 (C–H), 124.91 (C–H), 119.3 (C–H), 118.31 (C), 116.0 (J = 21.5 Hz, C–H), 76.5 (C–I).

6.1.2. General procedure for the Buchwald reaction coupling

2-(4-Fluorophenyl)-6-iodo-3-pyridin-4-ylimidazo[1,2-*a*]pyridine (415 mg, 1 mmol), copper (I) iodide (9.5 mg, 0.05 mmol), and potassium phosphate (425 mg, 2 mmol) were added to a screw-capped test tube. The tube was evacuated and back filled with argon (three times). Ethylene glycol (111 μL, 2 mmol), amine (1.2 mmol) and butanol (1 mL) were added successively by syringe at room temperature. The tube was sealed with a Teflon-lined cap and the reaction mixture was heated at 100 °C for 14 h. After cooling to room temperature, the suspension was diluted with a mixture of 1 mL of NH_4OH 30% and 20 mL of water, and then extracted with DCM. The organic layer was dried over anhydrous $MgSO_4$ and concentrated to dryness. The residue was chromatographed on alumina eluted with DCM and then a mixture of DCM–methanol (98–2).

6.1.2.1. 2-[2-(4-Fluorophenyl)-3-pyridin-4-ylimidazo[1,2-a]pyridin-6-ylamino]ethanol (**3a**).

M = 120 mg. Yield: 34.5%. Mp = 205 °C (déc). ^{1}H NMR (400.13 MHz, $CDCl_3$): 8.76 (d, J = 5.8 Hz, 2H, Pyr-3,5), 7.55 (d, J = 9.5 Hz, 1H, H-8), 7.53 (dd, J = 8.5–5.4 Hz, 2H, F-Ph-2,6), 7.39 (d, J = 5.8 Hz, 2H, Pyr-3,5), 7.32 (d, J = 1.4 Hz, 1H, H-5), 7.00 (t, J = 8.5 Hz, 2H, F-Ph-3,5), 6.89 (d, J = 9.5 Hz, 1H, H-7), 3.90 (t, J = 5.1 Hz, 2H, CH_2), 3.15 (t, J = 5.1 Hz, 2H, CH_2). ^{13}C NMR (100 MHz, $CDCl_3$): 162.5 (J = 255.6 Hz, C–F), 151.1 (C–H), 140.9 (C), 138.2 (C), 137.4 (C), 130.0 (J = 8 Hz, C–H), 129.6 (C), 129.1 (C), 127.2 (C), 124.5 (C–H), 121.0 (C–H), 118.1 (C–H), 115.5 (J = 21.1 Hz, C–H), 102.7 (C–H), 60.9 (CH_2), 46.5 (CH_2). Mass spectroscopy: m/z = 348. The spectra were acquired in MeOH as solvent with 10% DMSO.

6.1.2.2. 4-[2-(4-Fluorophenyl)-3-pyridin-4-ylimidazo[1,2-a]pyridin-6-ylamino]butan-1-ol (**3b**).

M = 186 mg. Yield: 49%. Mp = 200 °C. ^{1}H NMR (400.13 MHz, $CDCl_3$): 8.76 (d, J = 5.8 Hz, 2H, Pyr-2, 6), 7.54 (d, J = 9.8 Hz, 1H, H-8), 7.53 (dd, J = 8.8–5.4 Hz, 2H, F-Ph-2,6), 7.39 (d, J = 5.8 Hz, 2H, Pyr-3,5), 7.24 (d, J = 1.7 Hz, 1H, H-5), 7.00 (t, J = 8.8 Hz, 2H, F-Ph-3,5), 6.85 (dd, J = 9.5–2 Hz, 1H, H-7), 3.71 (t, J = 6 Hz, 2H, CH_2), 3.00 (t, J = 6.5 Hz, 2H, CH_2), 1.73 (m, 4H, $2CH_2$). ^{13}C NMR (100 MHz, $CDCl_3$): 162.5 (J = 252 Hz, C–F), 151.1 (CH), 142.1 (C), 138.5 (C), 137.3 (C), 130.0 (J = 7.7 Hz, C–H), 129.6 (C), 129.1 (C), 127.4 (C), 124.5 (C–H), 121.2 (C–H), 117.8 (C–H), 115.6 (J = 21.8 Hz, C–H), 101.9 (C–H), 62.4 (CH_2), 44.3 (CH_2), 30.2 (CH_2), 25.7 (CH_2). Mass spectroscopy: m/z = 377. The spectra were acquired in MeOH as solvent with 10% DMSO.

6.1.2.3. 6-[2-(4-Fluorophenyl)-3-pyridin-4-ylimidazo[1,2-a]pyridin-6-ylamino]hexan-1-ol (**3c**).

M = 126 mg. Yield: 31.2%. Mp = 200 °C. ^{1}H NMR (400.13 MHz, $CDCl_3$): 8.76 (d, J = 6 Hz, 2H, Pyr-2, 6), 7.54 (m, 3H, H-8, F-Ph-2,6), 7.39 (d, J = 6 Hz, 2H, Pyr-3,5), 7.22 (d, J = 1.7 Hz, H-5), 7.00 (t, J = 8.7 Hz, 2H, F-Ph-3,5), 6.84 (dd, J = 9.6–2 Hz, 1H, H-7), 3.67 (t, J = 6.5 Hz, 2H, CH_2), 3.42 (bs, 1H, NH), 2.96 (m, 2H, CH_2), 1.67 (m, 2H, CH_2), 1.60 (m, 2H, CH_2), 1.44 (m, 4H, $2CH_2$). ^{13}C NMR (100 MHz, $CDCl_3$): 162.5 (J = 246 Hz, C–F), 151.1 (C–H), 142.0 (C), 138.5 (C), 137.4 (C), 130.0 (J = 8 Hz, C–H), 124.6 (C–H), 121.0 (C–H), 120.6 (C), 118.2 (C), 117.8 (C–H), 115.5 (J = 21 Hz, C–H), 106.3 (C), 101.8 (C–H), 62.9 (CH_2), 44.4 (CH_2), 32.7 (CH_2), 29.2 (CH_2), 27.0 (CH_2), 25.7 (CH_2). Mass spectroscopy: m/z = 404. The spectra were acquired in MeOH as solvent with 10% DMSO.

6.2. Cell culture

The human myelomonocytic cell line, THP-1 (ECACC 88081201; Sophia-Antipolis, France) [45–47] was used. These non-adherent cells were grown in suspension in RPMI 1640 with glutamax™-I (Gibco, Eragny, France) and antibiotics (100 U/mL penicillin, 100 μg/mL streptomycin) (Gibco), supplemented with 10%(v/v) heat-inactivated fetal calf serum (Gibco). The THP-1 cells were incubated at 37 °C under a 5% CO_2/95% air atmosphere (v/v).

6.3. Vesicule preparation

L-α-Phosphatidylcholine from egg yolk (EPC) and synthetic *dimyristoyl phosphatidylcholine* (DMPC) were obtained from Sigma, la Verpillère, France. DMPC deuterated on both chains or

polar headgroup was purchased from Interchim, Montluçon, France.

6.4. Small unilamellar vesicles (SUV)

EPC in its chloroformic solution (100 mg/mL) was evaporated to a film and resuspended in pure D_2O to a final lipid concentration of 10 mM in 500 μL. SUV were formed by 1 h bath sonication. For drug containing SUV, the respective chloroformic solutions were mixed before lyophilization to a molar ratio of 1/10.

6.5. Multilayers vesicles (MLV)

DMPC in its chloroformic solution was evaporated to a film and resuspended in pure D_2O. The liposomes were formed by fast freezing and thawing cycles. The final lipid concentration was 50 mM and drug/lipid molar ratio was 1:5. For ^2H NMR experiments, lyophilized DMPC containing 20% phospholipids perdeuterated chains (DMPC-d_{54}) or on the *N*-trimethyl group of the choline polar head (DMPC-d_9) was resuspended in deuterium-depleted water.

6.6. NMR experiments

6.6.1. High resolution NMR

NMR experiments: ^1H NMR experiments were recorded at 296 K on a Bruker AM-400 spectrometer using a 4000 Hz spectral width, 32 K digitization points, a recycling delay of 2 s and a presaturation of the solvent resonances was used for all the experiments in aqueous medium.

^{31}C NMR experiments were recorded at 296 K on a Bruker AM-400 spectrometer using a 250 ppm spectral width, 64 K digitization points, a recycling delay of, 60° pulses of 5 μs and a composite pulse proton decoupling.

^{31}P and ^2H NMR experiments were performed at 162 and 61 MHz respectively. Phosphorus spectra were recorded using a dipolar echo sequence ($\pi/2$–t–π–t) [48] with a t value of 18 μs, a $-\pi/2$ pulse of 10 μs and a broadband two level proton decoupling. Phosphoric acid (85%) was used as external reference. Deuterium spectra were recorded by using a quadrupolar echo sequence ($\pi/2$–t–$\pi/2$–t) with a $\pi/2$ pulse of 8 μs, and a t value of 35 μs to form the echo. The free induction decay was shifted by fractions of the dwelling time to ensure that its effective time for the Fourier transform corresponds to the top of the echo [20]. The sample temperature was regulated within 1 °C by a BVT-1000 unit.

^2H NMR spectra treatment: in order to extract suitable quadrupolar splitting measurements ($\Delta\nu_Q$), the spectra were dePaked according to Bloom and coworkers.

6.6.2. HR-MAS

All HR-MAS experiments were performed on Bruker AVANCE-DMX-400 (proton frequency 400.13 MHz) using a Bruker HR-MAS probe head. Samples were loaded in zirconium oxide 4 mm cylindrical rotor with spherical insert (internal volume of 50 μl). Samples were spun at 4000 Hz.

NMR experiments. *^1H NMR* experiments were recorded at 16 K digitization points, a recycling delay of 1.5 s and a presaturation of the solvent resonances was used for all the experiments in aqueous medium.

6.7. Partition coefficient (log P)

log *P* was extracted from optical density measurements on performed at 285 nm on a Shimazu ER-3 spectrometer. References were solutions of identical concentration in octanol (O_1) and water (W_1) separately. After mixing and centrifugation of the two phases, similar measurements were then performed on the water (W_2) and the octanol (O_2) layers. The values for log *P* were finally derived from:

$$\log P = \log(W_2O_1/W_1O_2),$$

and controlled by numerical calculation (ACD-LAB reference), giving log *P* [**E1**] = 1.75; log *P* [**B1**] = 2.3; log *P* [**H1**] = 3.2.

6.8. Fluorescence measurements

A model SFM-25 spectrofluorimeter (Kontron Instruments) was used with the excitation and emission. Excitation and emission wavelengths were 344 and 434–427 nm respectively. The solution analyzed was prepared by dissolution of **3c** (the range 6.6 to 30 μmol/L) in the distilled water to give a final volume of 1 mL.

6.9. Spin label study (ESR) experiments

Effect of **3a**, **3b** and **3c** molecules on MLV fluidity was assessed by ESR spin label experiments. Two spin labels (Sigma France) were used: 5-nitroxide stearate (5 NS) and 16-nitroxide stearate (16 NS). This fatty acids self incorporate the MLV and the nitroxide groups provide information of motional freedom of the label in the system. So the former probes the superficial part of the membrane layer, the latter in its hydrophobic core [49].

The experiments were performed on MLV made with DMPC 50 mg/mL. Each molecule was added in 200 μL MLV solution to reach the final concentration of 1 mM and then labeled with 10 μL of spin label solution (5 NS 10^{-3} M or 16 NS 10^{-3} M). After 30 min incubation at room temperature, sample was transferred by capillarity in 20 μL Pyrex capillary tube. This tube was placed in a 3 mm diameter quartz holder, and inserted into the cavity of the ESR spectrometer.

The ESR spectra were recorded at different controlled temperature (294, 295, 296, 297, 298 and 299 K) with the following conditions: microwave power 10.00 mW, modulation frequency 100 kHz, modulation amplitude 2.05 G, receiver gain 2.5×10^5conversion time 81.92 ms, time constant 163.84 ms. Sweep range was 100 G with a central field value of 3435 G for 5 NS probe, and in the same condition except, modulation amplitude 1.03 G, receiver gain 10^5conversion time 40.96 ms, time constant 163.84 ms for 16 NS probe.

The complete membrane incorporation of the spin labels was ascertained by the absence on the spectra of the extremely resolved ESR lines corresponding to free rotating markers.

5 NS experimentations: the values of outer and inner hyperfine splitting were measured ($2T_{\|}$and $2T_{\perp}$respectively), on ESR spectra (Fig. 6-B), and order parameter *S* was calculated following the equation [50]:

$$S = 1.723 \times \frac{T_{//} - (T_{\perp} + C)}{T_{//} + 2(T_{\perp} + C)} \text{ with}$$

$$C = 1.4 - 0.053 \times \left(T_{//} - T_{\perp}\right)$$

The increase of the order parameter value means a decrease of local membrane fluidity.

16 NS experimentations: the changes in freedom motion of 16 NS were analyzed with the calculation of τ_c, the rotational correlation time. τ_c was calculated following the formula [51]:

$$T_c = K \times \Delta W_0 \left(\sqrt{(h_o/h_{-1})} - 1\right) \text{ With } K = 6.5 \times 10^{-10} \text{s G}^{-1}$$

In this formula, ΔW_0 is the peak-to-peak linewidth of the central line; h_0 and h_{-1} are the peak height of the central and high field lines respectively (Fig. 6-D).

The decrease of the rotational correlation time means a decrease of local membrane fluidity.

Acknowledgments

Thanks to Prof. Anny Han for helpful corrections, and to Sandrine Richard for cell culture.

References

[1] R. Craig, A. Larkin, A.M. Mingo, D.J. Thuerauf, C. Andrews, P.M. McDonough, C.C. Glembotski, J. Biol. Chem. 275 (2000) 23814–23824.
[2] F. Bazzoni, B. Beutler, N. Engl. J. Med. 334 (1996) 1717–1725.
[3] M. Feldmann, F.M. Brennan, R. Maini, Int. Rev. Immunol. 17 (1998) 217–228.
[4] S. Kumar, J. Boehm, J.C. Lee, Nat. Rev. Drug Discov. 2 (2003) 717–726.
[5] M.A. Palladino, F.R. Bahjat, E.A. Theodorakis, L.L. Moldawer, Nat. Rev. Drug Discov. 2 (2003) 736–746.
[6] S. Miwatashi, Y. Arikawa, E. Kotani, M. Miyamoto, K. Naruo, H. Kimura, T. Tanaka, S. Asahi, S. Ohkawa, J. Med. Chem. 48 (2005) 5966–5979.
[7] N.W. Freshney, L. Rawlinson, F. Guesdon, E. Jones, S. Cowley, J. Hsuan, J. Saklatvala, Cell 78 (1994) 1039–1049.
[8] J.C. Lee, J.T. Laydon, P.C. McDonnell, T.F. Gallagher, S. Kumar, D. Green, D. McNulty, M.J. Blumenthal, J.R. Heys, S.W. Landvatter, J.E. Strickler, M.M. McLaughlin, I.R. Siemens, S.M. Fisher, G.P. Livi, J.R. White, J.L. Adams, P.R. Youn, Nature 372 (1994) 739–746.
[9] T. Hunter, Cell 80 (1995) 225–236.
[10] S.K. Hanks, A.M. Quinn, T. Hunter, Science 241 (1988) 42–52.
[11] K. Ono, J. Han, Cell. Signalling 12 (2000) 1–13.
[12] S.K. Hanks, T. Hunter, FASEB J. 9 (1995) 576–596.
[13] C.M. Crews, A.A. Alessandrini, R.L. Erikson, Proc. Natl. Acad. Sci. U.S.A. 88 (1991) 8845–8849.
[14] J. English, G. Pearson, J. Wilsbacher, J. Swantek, M. Karandikar, S. Xu, M.H. Cobb, Exp. Cell Res. 253 (1999) 255–270.
[15] J.D. Ashwell, Nat. Rev. Immunol. 6 (2006) 532–540.
[16] Z. Chen, H. Seimiya, M. Naito, T. Mashima, A. Kizaki, S. Dan, M. Imaizumi, H. Ichijo, K. Miyazono, T. Tsuruo, Oncogene 18 (1999) 173–180.
[17] J. Raingeaud, S. Gupta, J.S. Rogers, M. Dickens, J. Han, R.J. Ulevitch, R.J. Davis, J. Biol. Chem. 270 (1995) 7420–7426.
[18] S. Bellon, M.J. Fitzgibbon, T. Fox, H.M. Hsiao, K.P. Wilson, Structure 7 (1999) 1057–1065.
[19] B.J. Canagarajah, A. Khokhlatchev, M.H. Cobb, E.J. Goldsmith, Cell 90 (1997) 859–869.
[20] C. Enguehard-Gueiffier, F. Fauvelle, J.C. Debouzy, A. Peinnequin, I. Thery, V. Dabouis, A. Gueiffier, Eur. J. Pharmacol. Sci. 24 (2005) 219–227.
[21] K.P. Wilson, P.G. McCaffrey, K. Hsiao, S. Pazhanisamy, V. Galullo, G.W. Bemis, M.J. Fitzgibbon, P.R. Caron, M.A. Murcko, M.S. Su, Chem. Biol. 4 (1997) 423–431.
[22] J. Campbell, C.J. Ciesielski, A.E. Hunt, N.J. Horwood, J.T. Beech, L.A. Hayes, A. Denys, M. Feldmann, F.M. Brennan, B.M. Foxwell, J. Immunol. 173 (2004) 6928–6937.
[23] J.F. Kerr, A.H. Wyllie, A.R. Currie, Br. J. Cancer 26 (1972) 239–257.
[24] T. Shimizu, E. Maeno, Y. Okada, Sheng Li Xue Bao 59 (2007) 512–516.
[25] M.B. Friis, C.R. Friborg, L. Schneider, M.B. Nielsen, I.H. Lambert, S.T. Christensen, E.K. Hoffmann, J. Physiol. 567 (2005) 427–443.
[26] J. Huot, F. Houle, S. Rousseau, R.G. Deschesnes, G.M. Shah, J. Landry, J. Cell Biol. 143 (1998) 1361–1373.
[27] J.C. Debouzy, V. Dabouis, S. Crouzy, C. Bachelet, A. Favier, A. Peinnequin, A. Gueiffier, Pharmazie 56 (2001) 125–132.
[28] J. Auwerx, Experientia 47 (1991) 22–31.
[29] J. Seelig, Q. Rev. Biophys. 10 (1977) 353–418.
[30] J.M. Neumann, A. Zachowski, S. Tran-Dinh, P.F. Devaux, Eur. Biophys. J. 11 (1985) 219–223.
[31] D.D. Lasic, Biochem. J. 256 (1988) 1–11.
[32] E.A. Dennis, A. Plückthun, in: Gorenstein (Ed.), Phosphorus 31P-NMR: Principles and Applications, Academic Press, London, 1984, pp. 423–480.
[33] D. Canet, J.C. Boubel, E. Soulas, La RMN, concepts, méthodes et applications Paris (2002).
[35] J.P. Douliez, A. Léonard, E.J. Dufourc, J. Phys.Chem. 100 (1996) 400–457.
[36] F. Fauvelle, J.C. Debouzy, S. Crouzy, M. Goschl, Y. Chapron, J. Pharm. Sci. 86 (1997) 935–943.
[37] E.J. Dufourc, C. Mayer, J. Stohrer, G. Althoff, G. Kothe, Biophys. J. 61 (1992) 42–57.
[38] J.C. Debouzy, J.M. Neumann, M. Hervé, D. Daveloose, J. Viret, R. Apitz-Castro, Eur. Biophys. J. 17 (1989) 211–216.
[39] A. Peinnequin, A. Piriou, J. Mathieu, V. Dabouis, C. Sebbah, R. Malabiau, J.C. Debouzy, Bioelectrochemistry 51 (2000) 157–161.
[40] P. Duchene, P. Papalexiou, J. Ramis, I. Izquierdo, G. Houin, Arzneimittelforschung 42 (1992) 861–863.
[41] J.C. Debouzy, A. Gueiffier, F. Fauvelle, H. Viols, E. Dejean, V. Neirinck, A. Peinnequin, C. Bachelet, B. Perly, J.P. Chapat, J. Pharm. Sci. 85 (1996) 200–205.
[42] M. Gorria, X. Tekpli, O. Sergent, L. Huc, F. Gaboriau, M. Rissel, M. Chevanne, M.T. Dimanche-Boitrel, D. Lagadic-Gossmann, Ann. N.Y. Acad. Sci. 1090 (2006) 108–112.
[43] D. Jourd'heuil, A. Aspinall, J.D. Reynolds, J.B. Meddings, Can. J. Physiol. Pharmacol. 74 (1996) 706–711.
[44] C. Enguehard, H. Allouchi, A. Gueiffier, S.L. Buchwald, J. Org. Chem. 68 (2003) 4367–4370.
[45] S. Tsuchiya, M. Yamabe, Y. Yamaguchi, Y. Kobayashi, T. Konno, K. Tada, Int. J. Cancer 26 (1980) 171–176.
[46] S. Tsuchiya, Y. Kobayashi, Y. Goto, H. Okumura, S. Nakae, T. Konno, K. Tada, Cancer Res. 42 (1982) 1530–1536.
[47] K.M. Skubitz, S. Pessano, L. Bottero, D. Ferrero, G. Rovera, J.T. August, J. Immunol. 131 (1983) 1882–1888.
[48] T. Mavromoustakos, I. Daliani, J. Matsoukas, Biomed. Health Res. 22 (1999) 13–24.
[49] J.C. Debouzy, D. Crouzier, A. Gadelle, Ann. Pharm. Fr. 65 (2007) 331–341.
[50] B.J. Gaffney, in: R.J. Berliner (Ed.), Spin Labelling: Theory and Applications, Academic Press, New York London, 1976, pp. 567–571.
[51] A. Gornicki, A. Gutsze, Acta Biochim. Pol. 47 (2000) 963–971.